A novel spontaneous mutation of *Irs1* in mice results in hyperinsulinemia, reduced growth, low bone mass and impaired adipogenesis

Victoria E DeMambro, Masanobu Kawai[1], Thomas L Clemens[2], Keertik Fulzele[3], Jane A Maynard, Caralina Marín de Evsikova, Kenneth R Johnson, Ernesto Canalis[4], Wesley G Beamer, Clifford J Rosen[1] and **Leah Rae Donahue**

The Jackson Laboratory, 600 Main Street, Bar Harbor, Maine 04609, USA
[1]Medical Center Research Institute, Scarborough, Maine 04074, USA
[2]John Hopkins University, Baltimore, Maryland 21287, USA
[3]Massachusetts General Hospital, Boston, Massachusetts 02114, USA
[4]Department of Research, Saint Francis Hospital and Medical Center, Hartford, Connecticut 06105, USA
(Correspondence should be addressed to V E DeMambro; Email: victoria.demambro@yahoo.com)

Abstract

A spontaneous mouse mutant, designated 'small' (*sml*), was recognized by reduced body size suggesting a defect in the IGF1/GH axis. The mutation was mapped to the chromosome 1 region containing *Irs1*, a viable candidate gene whose sequence revealed a single nucleotide deletion resulting in a premature stop codon. Despite normal mRNA levels in mutant and control littermate livers, western blot analysis revealed no detectable protein in mutant liver lysates. When compared with the control littermates, $Irs1^{sml}/Irs1^{sml}$ ($Irs1^{sml/sml}$) mice were small, lean, hearing impaired; had 20% less serum IGF1; were hyperinsulinemic; and were mildly insulin resistant. $Irs1^{sml/sml}$ mice had low bone mineral density, reduced trabecular and cortical thicknesses, and low bone formation rates, while osteoblast and osteoclast numbers were increased in the females but not different in the males compared with the $Irs1^{+/+}$ controls. *In vitro*, $Irs1^{sml/sml}$ bone marrow stromal cell cultures showed decreased alkaline phosphatase-positive colony forming units (pre-osteoblasts; CFU-AP+) and normal numbers of tartrate-resistant acid phosphatase-positive osteoclasts. $Irs1^{sml/sml}$ stromal cells treated with IGF1 exhibited a 50% decrease in AKT phosphorylation, indicative of defective downstream signaling. Similarities between engineered knockouts and the spontaneous mutation of $Irs1^{sml}$ were identified as well as significant differences with respect to heterozygosity and gender. In sum, we have identified a spontaneous mutation in the *Irs1* gene associated with a major skeletal phenotype. Changes in the heterozygous $Irs1^{+/sml}$ mice raise the possibility that similar mutations in humans are associated with short stature or osteoporosis.
Journal of Endocrinology (2010) **204,** 241–253

Introduction

Insulin and insulin-like growth factor 1 (IGF1) are critical regulators of growth and metabolism in virtually all mammals. Insulin deficiency syndromes, such as diabetes mellitus type 1 (type I DM) and low IGF1 levels from GH deficiency or resistance, are associated with reduced bone mineral density (BMD) and heightened fracture risk (Garnero *et al.* 2000, Janghorbani *et al.* 2006, 2007, Räkel *et al.* 2008). GH deficiency and hence IGF1 deficiency in children and adults impair peak bone acquisition and are associated with an increased prevalence of fractures in adulthood (Vestergaard *et al.* 2002, Mukherjee *et al.* 2004, Giustina *et al.* 2008). Similarly, a spontaneous recessive mutation in GHRH also results in low areal BMD (aBMD) in mice and humans (Donahue & Beamer 1993, Godfrey *et al.* 1993, Maheshwari *et al.* 1998, Baumann 1999). Studies using genetically engineered mice have reinforced the importance of the IGF1 regulatory system in skeletal development. For example, global *Igf1* gene deletion causes a dramatic skeletal phenotype characterized by impaired bone formation and bone resorption (Liu *et al.* 1993, Bikle *et al.* 2001, He *et al.* 2006, Wang *et al.* 2006). Conditional targeted deletion of the type I IGF receptor (*Igf1r*) in osteoblasts causes a profound reduction in trabecular bone volume and osteoblast function, and changes in mineralization lag time (Zhang *et al.* 2002). Furthermore, engineered knockout and transgenic overexpression of several IGF-binding proteins induce marked changes in bone turnover and bone mass (Silha *et al.* 2003, Zhang *et al.* 2003, Atti *et al.* 2005, Ben Lagha *et al.* 2006, DeMambro *et al.* 2008). Likewise, hepatic-specific deletion of *Igf1* (Yakar *et al.* 1999) or global deletion of the acid-labile

DOI: 10.1677/JOE-09-0328
0022–0795/10/0204–241
Online version via http://www.endocrinology-journals.org

subunit (*Igfals*) in mice promotes marked thinning of the cortical bone compartment, despite minimal changes in linear growth (Yakar *et al.* 2009). Hence, skeletal and circulating IGF1 are essential for optimal peak bone acquisition.

Insulin and IGF1 initiate a chain of intracellular responses and signaling cascades upon binding to tyrosine kinase receptors (IR and *Igf1r*). The first substrates phosphorylated after ligand binding are the insulin receptor substrate (IRS) proteins. Once phosphorylated by their cognate receptors, these substrates bind to proteins containing Src homology-2 domains, which in turn activate a variety of signaling pathways, including activation of phosphatidylinositol 3-kinase and mitogen-activated protein kinase (Lienhard 1994, White 2003, Niu & Rosen 2005). These intracellular signaling pathways are essential for bone acquisition, since they impact the recruitment, differentiation, and death of osteoblasts (Cornish *et al.* 1996, Niu & Rosen 2005). Deletion of *Irs1* (either the $Irs1^{tm1Tka}$ or the $Irs1^{tm1Jos}$ allele) on a mixed B6/CBA hybrid mouse background results in growth retardation; however, both female and male mice are relatively healthy and fertile (Araki *et al.* 1994, Tamemoto *et al.* 1994). Adult $Irs1^{tm1Tka}/Irs1^{tm1Tka}$ ($Irs1^{tm1Tka/tm1Tka}$) mice have low aBMD and delayed fracture healing, with reductions in osteoblast and osteoclast numbers and function, resulting in decreased bone turnover. These null mice also exhibit impaired anabolic response to intermittent parathyroid hormone administration (Ogata *et al.* 2000, Hoshi *et al.* 2004, Shimoaka *et al.* 2004, Yamaguchi *et al.* 2005). Both the $Irs1^{tm1Tka/tm1Tka}$ and the $Irs1^{tm1Jos}/Irs1^{tm1Jos}$ ($Irs1^{tm1Jos/tm1Jos}$) mice have high serum insulin levels and are insulin resistant despite a lean phenotype, but circulating IGF1 levels were reported not to differ significantly from those of the controls (Araki *et al.* 1994, Tamemoto *et al.* 1994, Shirakami *et al.* 2002). Thus, several animal models have confirmed that insulin and IGF1 signaling are critical for skeletal acquisition and maintenance.

There are no reports of a spontaneous mutation in the *Irs1* gene leading to complete loss of function in mice or in humans. However, there are numerous studies on humans demonstrating polymorphisms in the *Irs1* gene associated with metabolic disease, some of which induce amino acid changes and variable responsiveness to insulin and/or IGF1 signaling (Imai *et al.* 1994, Ura *et al.* 1996, Le Fur *et al.* 2002). The most common polymorphism, the G972R variant, has been associated with type II diabetes mellitus (Almind *et al.* 1993, Sesti 2000, Tok *et al.* 2006). In contrast, there is no data examining the relationship between these polymorphisms and BMD or fracture risk.

Recently, in the Mouse Mutant Resource at The Jackson Laboratory, we discovered a small mouse phenotype that arose as a spontaneous autosomal recessive mutation on a congenic C3.SW-$H2^b$/SnJ inbred background. Molecular genetic studies revealed that this mutation, designated small (allele symbol *sml*), was due to a frameshift mutation in the *Irs1* gene. This report details the molecular and phenotypic characterization of this mutant and the cellular changes that occur in response to altered IRS-1 signaling. Findings from this study add to insights gained from previous work using genetic engineering, and raise important questions about the inter-relationship between the IGF1 regulatory system and bone acquisition.

Materials and Methods

Mouse husbandry

The $Irs1^{sml}$ allele is a spontaneous mutation that occurred in an inbred C3.SW-$H2^b$/SnJ mouse strain. All mice used in this study were produced and maintained in our research colony at The Jackson Laboratory (Bar Harbor, ME, USA). Mice were housed in groups of 4 or 5 of the same sex within polycarbonate boxes of 324 cm^2 in area on sterilized shavings of Northern White Pine. Colony environmental conditions included 14 h light:10 h darkness cycles, with free access to acidified water (pH 2·5 with HCl to retard bacterial growth) and irradiated NIH-31 diet containing 6% fat, 19% protein, Ca:P 1·15:0·85, plus vitamin and mineral fortified (Purina Mills International, Gray Summit, MO, USA). All studies were conducted using groups of mutant, heterozygous, and wild-type male and female mice. All procedures involving mice were reviewed and approved by the Institutional Animal Care and Use Committee of The Jackson Laboratory.

Genetic mapping

To map the *sml* mutation, 204 F_2 mice were produced from an intercross between (C3.SW-$H2^b$/SnJ-*sml*×CAST/Ei) F_1 hybrid mice. Genomic DNA from F_2 mice was prepared and genotyped using Mit marker primer pairs as described previously (Gagnon *et al.* 2006). The *sml* mutation was mapped utilizing recombination frequencies and the Map Manager Program (Manly *et al.* 2001).

Sequencing of the Irs1 *gene*

PCR primers used to amplify exons 1 and 2 of the mouse *Irs1* gene for sequence comparisons between mutant and control are given in Table 1. PCR conditions were described previously (Gagnon *et al.* 2006). PCR-amplified products were purified using the Qiaquick PCR Purification Kit (Qiagen Inc). DNA was sequenced using an Applied Biosystems 373A DNA Sequencer (Applied Biosystems, Foster City, CA, USA). The same primers that were used for PCR amplification were also used for sequencing.

Genotyping of the $Irs1^{sml}$ *colony*

To genotype this mouse colony, we recognized that the deletion of the one adenine nucleotide in exon 1 created a restriction enzyme recognition site, which Taq1 recognizes (T-CGA). We designed primers (*Irs1* F 5′-CAA GGA GGT

Table 1 *Irs1* gene amplification and sequencing primers

	Primer sequence 5′ to 3′	Product size
E1-1F	GACTGGGGGAGACATAGTCC	804
E1-1R	TCCAGAGGAGCAAAACACGTGA	
E1-2F	CCTTTGCCCGATTATGCAG	794
E1-2R	TGCTCGAGTCCGATGTAGG	
E1-3F	AGTACCAGTGGCCATGGCT	856
E1-3R	CCTTTGCCCGATTATGCAG	
E1-4F	TCATTAACCCCATCAGACGC	930
E1-4R	GTGCTAGGGCTCACAGGACT	
E1-5F	CAACAGCAGCAGCAGTCTTC	818
E1-5R	AGGAGACATGGGCATATAGCC	
E1-6F	GAGCAGGGGCTGCAGTAG	826
E1-6R	CTGTTGGTCTGTGCAGCTGT	
E1-7F	GGAAGGGTCAGGGTACACAG	642
E1-7R	CTTGAGTGTCTGCGCGAAT	
E1-2F	AAAATGTAGCTTTCATTACAGCACA	583
E2-1R	AATACGGAGAGCTCACCCCT	
E2-2F	TTCATACATTGCCTCCGAGA	725
E2-2R	CTCTCCACCCAACATGAACA	
E2-3F	CCTACCTTGTGTGTTCTGGGA	433
E2-3R	CAAATTCTAAGCCGACACTTG	

CTG GCA GGT TA-3′ and *Irs1* R 5′-CCC ACC TCG ATG AAG AAG AA-3′) to amplify the region of interest and then digested them with Taq1 restriction enzyme as per the manufacturer's instructions. The digested products yielded a control band of 190 bp, with a mutant band of 171 bp.

Quantitative real-time PCR

RNA was extracted from the femurs of four 8-week-old $Irs1^{sml/sml}$ and $Irs1^{+/+}$ control mice as described previously (DeMambro *et al.* 2008). Briefly, femurs were isolated and snap frozen in liquid nitrogen, and RNA was then isolated using the Total RNA isolation system (Promega) as per the manufacturer's instructions. DNA was then removed from the RNA samples using the DNA-free DNase Treatment & Removal Reagents (Ambion, Inc., Austin, TX, USA). RNA quality and quantity were assessed using an Agilent bioanalyzer (Caliper Technologies Corp., Hopkinton, MA, USA). Four hundred nanograms of RNA were then converted to cDNA in a reverse transcription reaction using the MessageSensor RT Kit (Ambion, Inc.) and random decamers as primers. The cDNA was then diluted 1:5 with water. Quantification of mRNA expression was carried out using an iQ SYBR Green Supermix in a iQ5 thermal cycler and detection system (Bio-Rad). *GAPDH* was used as an internal standard control gene for all quantifications. Primer sequences used in this study are as follows: *RANKL* (forward: 5′-TAC TTT CGA GCG CAG ATG GAT-3′ and reverse: 5′-CTG CGT TTT CAT GGA GTC TCA-3′), *osteoprotegerin* (forward: 5′-TCC GGC GTG GTG CAA G-3′ and reverse: 5′-AGA ACC CAT CTG GAC ATT TTT TG-3′), and *GAPDH* (forward: 5′-TGA ACG GGA AGC TCA CTG G-3′ and reverse: 5′-TCC ACC ACC CTG TTG CTG TA-3′).

Western blotting

Mouse livers were collected, frozen in liquid nitrogen, and stored at −80 °C until processing. Total cellular protein lysates were prepared in a buffer consisting of 50 mM Tris base (pH 8·2), 150 mM NaCl, 1% Igepal, and complete protease inhibitor cocktail tablets (Roche) for 30 min at 4 °C, followed by centrifugation at 10 000 ***g*** for 20 min at 4 °C. For immunoprecipitation, cell lysates were incubated with a rabbit anti-C-terminus IRS-1 antibody (Upstate #06-248, Millapore, Billerica, MA, USA) for 1 h at 4 °C. The immunocomplexes were then collected using an Immunoprecipitation Kit Protein A (#1719394 Roche) as per the manufacturer's instructions. Proteins were resolved on 10% SDS-polyacrylamide gels and transferred to polyvinylidene fluoride (PVDF) membranes (Millipore). Membranes were blocked with 5% non-fat dry milk (Bio-Rad), and were then incubated with the same anti-C-terminus IRS-1 antibody followed by a HRP-conjugated donkey anti-rabbit antibody (Santa Cruz #sc-2317). Signal was detected using an enhanced chemiluminescence kit (Amersham).

The calvarial cells post treatment were washed twice with ice-cold PBS and resuspended in a lysis radioimmunoprecipitation assay buffer supplemented with protease and phosphatase inhibitors (Sigma–Aldrich). Cell lysates were homogenized by rotating at 4 °C for 30 min and were then centrifuged at 10 000 ***g*** for 20 min at 4 °C. Protein concentrations were measured in the supernatant using Bradford's reagent (Bio-Rad). Proteins were resolved on 10% SDS-polyacrylamide gels and transferred to PVDF membranes. Membranes were incubated with antibodies for phosphorylated AKT (pAKT; Cell Signaling #9271, Danvers, MA, USA) or total AKT (tAKT; Cell Signaling #9272) followed by HRP-conjugated goat anti-rabbit antibody (Cell Signaling #7074). In a separate set of experiments, calvarial cells post treatment were immunoprecipitated with an IRS-2 (Millipore # 06-506) antibody subjected to SDS-PAGE as described above and were then incubated with a phosphotyrosine-specific antibody (Millipore #05-321).

Assessment of hearing by auditory brainstem response

Groups of female and male $Irs1^{sml/sml}$ and littermate $Irs1^{+/sml}$ mice (n=7–10) between 8 and 12 weeks of age were anesthetized with Avertin (tribromoethanol stabilized in tertiary amyl hydrate) given at a dose of 5 mg tribromoethanol/10 g body weight. Body temperature was maintained at 37–38 °C by placing the mice on an isothermal pad in a sound-attenuating chamber. Sub-dermal needles were used as electrodes, which were inserted at the vertex and ventrolaterally to each ear. Stimulus presentation, auditory brainstem response (ABR) acquisition, equipment control, and data management were coordinated using the computerized Intelligent Hearing Systems (IHS, Miami, FL, USA). A pair of high frequency transducers were coupled with the IHS to

generate specific acoustic stimuli. Clicks and 8, 16, and 32 kHz tone bursts were respectively channeled through plastic tubes into the animals' ear canals. The amplified brainstem responses were averaged by a computer and displayed on the computer screen. Auditory thresholds were obtained for each stimulus by reducing the sound pressure level at 10 dB steps and finally at 5 dB steps up and down to identify the lowest level at which an ABR pattern can be recognized (Gagnon *et al.* 2006).

Sample collection for phenotypic studies

For body composition and bone phenotyping (dual energy X-ray absorptiometry (DEXA), pQCT, and micro-computed tomography (MicroCT)), groups of female and male $Irs1^{sml/sml}$, littermate $Irs1^{+/sml}$, and $Irs1^{+/+}$ control mice ($n=10$) were necropsied and measured at 4, 8, 12, and 16 weeks of age. All time points showed the same pattern and statistical significance, thus for the simplicity of presentation, only the 16-week data are reported here. For each mouse, whole body weight was recorded, whole body DEXA scans were gathered, and tissue samples were collected. Skeletal preparations were prepared as described previously (Beamer *et al.* 2007, DeMambro *et al.* 2008). Serum was harvested from the whole blood collected at necropsy and was stored at −20 °C until assayed for hormones.

PIXImus for areal BMD

Groups of $Irs1^{sml/sml}$, littermate $Irs1^{+/sml}$, and $Irs1^{+/+}$ control female and male mice were measured at 4, 8, 12, and 16 weeks ($n=10$) for lean muscle mass, fat, and bone mineral using the PIXImus dual-energy X-ray densitometer (GE-Lunar, Madison, WI, USA). The PIXImus was calibrated daily with a mouse phantom provided by the manufacturer. Mice were placed ventral side down with each limb and tail positioned away from the body. Full body scans were obtained, and X-ray absorptiometry data were gathered and processed with the manufacturer's supplied software (Lunar PIXImus 2, version 2.1). The head was specifically excluded from all analyses due to concentrated mineral in skull and teeth.

pQCT for volumetric BMD bone densitometry

Volumetric BMD (vBMD) was measured on the left femur from groups ($n=10$) of female and male $Irs1^{sml/sml}$, littermate $Irs1^{+/sml}$, and $Irs1^{+/+}$ control mice at 4, 8, 12, and 16 weeks of age. Isolated femur lengths were measured with digital calipers (Stoelting, Wood Dale, IL, USA), and femurs were then measured for density using the SA Plus densitometer (Orthometrics, White Plains, NY, USA). Calibration of the SA Plus instrument was performed daily, and femurs were analyzed as described previously (DeMambro *et al.* 2008).

MicroCT40

Femurs from female and male $Irs1^{sml/sml}$, littermate $Irs1^{+/sml}$, and $Irs1^{+/+}$ control mice were scanned using MicroCT40 (Scanco Medical AG, Bassersdorf, Switzerland) to evaluate trabecular bone volume fraction and microarchitecture in the metaphyseal region of the distal femur. In addition, cortical thickness data were obtained at the mid-shaft. The MicroCT40 unit was calibrated weekly, and femurs were scanned under conditions described previously (DeMambro *et al.* 2008).

Bone histomorphometry

To determine whether the *in vivo* histomorphometry differences seen between the $Irs1^{sml/sml}$ and the $Irs1^{tm1Tka/tm1Tka}$ mice were the result of gender differences, we studied groups of $Irs1^{sml/sml}$ and $Irs1^{+/+}$ females and males ($n=6$) at 13 weeks of age. Mice were injected with 20 mg/kg calcein i.p. and with 50 mg/kg demeclocycline 7 days later. Mice were sacrificed 48 h following the demeclocycline injection. Femurs were then analyzed as described previously (DeMambro *et al.* 2008). A separate experiment in which $Irs1^{sml/sml}$ *and* $Irs1^{+/sml}$ females were evaluated was then used for comparison with the $Irs1^{+/+}$ females for the presence of any heterozygous effects. The terminology and units used are those recommended by the Histomorphometry Nomenclature Committee of the American Society for Bone and Mineral Research (Parfitt *et al.* 1987).

Osteoblast and osteoclast cultures

Bone marrow cells were harvested from femurs and tibias of 8-week-old mice. Osteoclast-like cells were generated by plating bone marrow stromal cells at 10×10^6/well on six-well plates in α-MEM (Invitrogen) and 10% fetal bovine serum (FBS). Osteoclast-like cells were generated by plating bone marrow stromal cells at 1×10^6 cells/well in 48-well plates in α-MEM supplemented with 10% FCS and M-CSF (30 ng/ml, PeproTech Inc., Rocky Hill, NJ, USA) and RANKL (50 ng/ml PeproTech). Cultures were maintained, fixed, stained, and analyzed as described previously (DeMambro *et al.* 2008).

Mouse calvarial osteoblasts were harvested from 3- to 6-day-old pups using standard methods (http://skeletalbiology.uchc.edu/30_ResearchProgram/304_gap/index.htm). The cells were cultured in 10% FBS α-MEM to 90% confluence and were then serum starved in 0·1% FBS for 24 h to reduce cellular activity to quiescent levels. Cells were treated with insulin (100 nM) or IGF1 (100 ng/ml) for 15 min and were then harvested for western blot analysis. Data presented for cell culture experiments correspond to three independent experiments with at least three replicate cultures within each experiment.

Table 2 Auditory brainstem response in *Irs1*$^{+/sml}$ and *Irs1*$^{sml/sml}$ mice

	+/*sml* Males	*sml/sml* Males	+/*sml* Females	*sml/sml* Females
	n=7	*n*=9	*n*=10	*n*=12
Click	34·3±1·7	51·1±5·9*	33·5±0·8	53·8±5·2*
8 kHz	27·9±4·6	50·0±6·5*	23·5±1·1	55·0±6·2*
16 kHz	15·7±4·6	34·4±7·1*	16·0±1·0	36·7±5·3*
32 kHz	40·0±2·7	61·7±6·1*	41·0±1·0	66·3±5·4*

*$P<0·05$ +/*sml* versus *sml/sml*.

Serum IGF1 and insulin

Serum IGF1 levels were measured by RIA (ALPCO, Windham, NH, USA) as reported previously (Rosen *et al.* 2000, 2004, Delahunty *et al.* 2006). Serum insulin was measured by RIA (LINCO Research, St Charles, MO, USA) as per the manufacturer's instructions. The sensitivities of the assays were 0·01 ng/ml for IGF1 and 0·1 ng/ml for insulin. The intra-assay coefficient of variation for the assays was 4·5–4·6%. All samples were analyzed within the same assay.

Glucose and insulin tolerance tests

Female and male *Irs1*$^{sml/sml}$, *Irs1*$^{+/sml}$, and *Irs1*$^{+/+}$ mice were tested at 8 and 12 weeks of age for glucose and insulin tolerance. For the glucose tolerance test (GTT), mice were placed in a clean cage with water and fasted overnight (16 h). A 1 g/kg dose of glucose was administered i.p., and blood glucose levels were measured at 0, 20, 40, 60, and 120 min post injection. For the insulin tolerance test (ITT), mice were fed *ad libitum* and injected i.p. with insulin at a dose of 1 U/kg. Glucose levels were then measured at 0, 20, 40, 60, and 120 min post injection.

Glucose levels were measured using the OneTouch Ultra Glucometer (LifeScan, Inc., Milpitas, CA, USA) as per the manufacturer's instructions (Messier & Kent 1995, Weitgasser *et al.* 1999). In a separate experiment, we verified the accuracy and precision of the most recently manufactured OneTouch Ultra portable glucometers against Beckman Synchron CX5 Delta Clinical System (Beckman Coulter, Brea, CA, USA) using blood samples from 8- to 12-week-old C57BL6/J mice ($n=16$). This comparison confirmed that glucose levels reported using portable glucometers correlated highly ($r^2=0·92$) against the glucose levels reported by the Beckman Synchron CX5 Delta Clinical System (data not shown).

Statistical assessment

Statistical tests were performed using JMP version 6.0 software (SAS, Cary, NC, USA) and StatView version 5.0.1 software (SAS). For the DEXA, pQCT, and MicroCT40 data, differences among *Irs1*$^{sml/sml}$, *Irs1*$^{+/sml}$, and *Irs1*$^{+/+}$ mice were taken into account by including body weight and femur length as covariates in an ANCOVA model. Neither covariate was found to contribute to any of the mutant phenotypes. Data are expressed as mean±S.E.M. in all figures. Differences between means were tested by ANOVA, with significance being declared when a $P\leq0·05$ was observed.

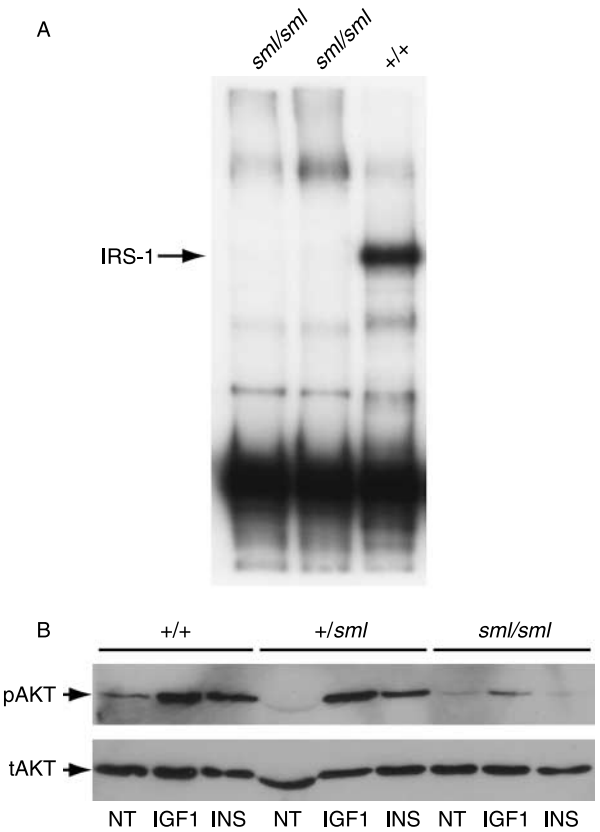

Figure 1 Western blots of IRS-1 (A) and AKT (B). (A) Liver lysates from *Irs1*$^{sml/sml}$ mice (lanes 1–2) and an *Irs1*$^{+/+}$ control (lane 3) were immunoprecipitated with an IRS-1 C-terminus-specific antibody as described in the Materials and Methods. Following SDS-PAGE, the amount of IRS-1 was determined by immunoblotting. The arrow denotes the position of the IRS-1 band which is lacking in *Irs1*$^{sml/sml}$ lysates. (B) Mouse calvarial osteoblast cultures from *Irs1*$^{sml/sml}$, *Irs1*$^{+/sml}$, and *Irs1*$^{+/+}$ mice were treated with IGF1 (IGF1) and insulin (INS) or were given no treatment (NT), harvested, and lysed as described in the Materials and Methods. Following SDS-PAGE, membranes were immunoblotted for phosphorylated AKT (pAKT) and total AKT (tAKT).

Results

History of the Irs1^{sml} *mutation*

The original *Irs1*^{sml} mutant was backcrossed to the C3.SW-*H2*^{b}/SnJ parental strain resulting in no mutants being observed in the F1 progeny. However, the expected Mendelian ratio of 3:1 unaffected:affected for a recessive mutation was observed in the F2 progeny. Gross histological examination found no lesions in any major organs other than decreased size (data not shown). No eye defects were detected. Hearing was assessed by ABR, and both male and female mutant mice exhibited significantly higher thresholds at 8, 16, and 32 kHz than the control littermates, indicative of hearing impairment in these mice (Table 2). Histological examination of the inner ear found no obvious defects.

Genetic mapping and mutation analysis of the Irs1^{sml} *mutation*

The F2 progeny from an intercross with CAST/Ei were used to map the *sml* mutation to chromosome 1 between *D1Mit216* (79·8 Mb) and *D1Mit440* (90·7 Mb). Analysis of 204 F2 mice (408 meioses) positioned *sml* between *D1Mit216* (79·8 Mb, 1·23% recombination) and *D1Mit440* (90·7 Mb, 2·45% recombination). *Irs1* is located at 82·2 Mb, and was considered a prime candidate for this mutation because of the smaller size of a knockout model reported previously (see Introduction).

Genomic DNA from *Irs1*$^{sml/sml}$ mice and *Irs1*$^{+/+}$ controls was analyzed for the *Irs1* gene by PCR amplification using overlapping primer pairs (Table 1) and sequence analysis. We discovered a deletion of one adenine nucleotide in exon 1 at position 1559 bp. This deletion results in a frameshift mutation changing a glutamine to an arginine residue, which produces a premature stop codon, predicted to result in a truncated protein of 211 amino acids instead of the full-length 1233-amino acid protein.

To confirm this mutation, we recognized that the deletion of the one adenine nucleotide created a restriction enzyme recognition site, which Taq1 recognizes (T-CGA). Thus, the region of interest was amplified, and Taq1 digestion yielded the control product of 190 bp, with a mutant product of 171 bp, confirming the deletion. Quantification of *Irs1* mRNA levels by real-time RT-PCR revealed no differences in expression between the *Irs1*$^{+/+}$ and the *Irs1*$^{sml/sml}$ mice (data not shown). Western blot analysis of proteins from the livers of the *Irs1*$^{sml/sml}$ and *Irs1*$^{+/+}$ control mice using a C-terminus-specific IRS-1 antibody revealed that the *Irs1*$^{sml/sml}$ mice had no detectable IRS-1 protein (Fig. 1A).

Body composition by DEXA

Homozygous male and female *Irs1*$^{sml/sml}$ mice are phenotypically recognizable at ∼2 weeks of age by their smaller size and thin short tails, a condition that persists throughout their lives despite normal GH levels. After weaning, mutants are ∼60% the size of their *Irs1*$^{+/sml}$ control littermates, including a 20% reduction in tail length (Table 3). Whole body DEXA analysis at 16 weeks of age revealed that *Irs1*$^{sml/sml}$ male and female mice had reduced percent fat and aBMD compared with the *Irs1*$^{+/+}$ controls. *Irs1*$^{+/sml}$ heterozygous mice had lower body weight, aBMD, and percent fat than the *Irs1*$^{+/+}$ mice, but these parameters were greater than those of the *Irs1*$^{sml/sml}$ mutants (Table 3).

Skeletal microstructure by pQCT and MicroCT

Analysis of femurs isolated from 16-week-old *Irs1*$^{+/+}$, *Irs1*$^{+/sml}$, and *Irs1*$^{sml/sml}$ mice revealed that *Irs1*$^{sml/sml}$ male and female mice had significant reductions in femur length, with an overall reduction in vBMD as measured by pQCT when compared with the *Irs1*$^{+/+}$ control mice. *Irs1*$^{sml/sml}$ femurs also exhibited a reduction in cortical thickness as well as in periosteal circumference (Table 3). MicroCT analysis confirmed the reduction in cortical thickness with a smaller cortical bone area/total area (percent BA/TA). The distal femoral trabecular bone exhibited a significant reduction in

Table 3 Body composition and bone phenotype of *Irs1*$^{+/+}$, *Irs1*$^{+/sml}$, and *Irs1*$^{sml/sml}$ mice by DEXA, pQCT, and micro-computed tomography at 16 weeks of age

	+/+ Males	+/*sml* Males	*sml/sml* Males	+/+ Females	+/*sml* Females	*sml/sml* Females
Body weight	37·9±1·0	32·3±0·9*	16·5±0·7†,‡	35·6±1·1	31·9±1·2*	15·4±0·4†,‡
F. length (mm)	15·58±0·07	15·08±0·11*	12·55±0·04†,‡	15·47±0·09	14·99±0·11*	12·83±0·06†,‡
Percent fat	32·8±0·8	28·5±1·2*	20·6±1·9†,‡	39·9±1·4	35·3±1·3*	16·8±1·4†,‡
aBMD (g/cm^2)	0·057±0·001	0·05±0·001*	0·039±0·001†,‡	0·058±0·001	0·049±0·001*	0·038±0·001†,‡
vBMD (mm/cm^3)	0·83±0·01	0·73±0·01*	0·65±0·01†,‡	0·86±0·01	0·76±0·01*	0·66±0·01†,‡
Peri. circ. (mm)	4·79±0·03	4·62±0·04*	3·73±0·02†,‡	4·70±0·02	4·28±0·03*	3·61±0·03†,‡
BA/TA (%)	79·0±0·7	75·2±1·1*	71·3±0·8†,‡	81·3±0·4	79·2±0·6*	73·9±0·4†,‡
CortTh (mm)	37·14±0·66	33·26±0·75*	25·14±0·44†,‡	38·32±0·43	34·14±0·47*	25·3±0·20†,‡
BV/TV (%)	22·0±1·4	21·0±0·8	15·4±0·9†,‡	28·3±1·2	26·2±0·6	7·5±0·7†,‡
TbN (/mm)	4·4±0·1	4·8±0·1	5·3±0·2†,‡	4·2±0·1	4·1±0·1	2·8±0·2†,‡
TbTh (mm)	73·9±2·7	66·3±1·3*	49·3±0·7†,‡	89·6±1·1	85·5±1·7*	51·8±0·8†,‡

n=10, *P<0·05 ++ versus +/*sml*, $^{\dagger}P$<0·0001 +/+ versus *sml/sml*, $^{\ddagger}P$<0·0001 +/*sml* versus *sml/sml*. F. length, femur length; Peri. circ., periosteal circumference; BA/TA, bone area/total area; CortTh, cortical thickness; BV/TV, bone volume/total volume; TbN, trabecular number; TbTh, trabecular thickness.

Table 4 Histomorphometry of *Irs1*$^{+/+}$ and *Irs1*$^{sml/sml}$ distal femurs at 13 weeks of age

	+/+ Males	*sml/sml* Males	+/+ Females	*sml/sml* Females
Percent BV/TV	12·09±0·63	7·80±0·08*	13·47±1·63	6·94±1·24*
Nob/BPm (/mm)	28·00±1·23	29·82±2·12	27·28±1·52	31·83±1·05*
Noc/BPm (/mm)	3·70±0·37	4·32±0·77	3·90±0·35	5·75±0·38*
ES/BS (%)	12·5±1·29	13·58±1·69	12·87±1·22	17·06±0·67*
MS/BS (%)	6·89±0·51	2·41±0·38*	7·14±0·84	4·10±0·32*
MAR (μm/day)	0·441±0·026	0·290±0·024*	0·640±0·027	0·439±0·047*
BFR/BS ($\mu m^3/\mu m^2$ per day)	0·031±0·003	0·007±0·001*	0·046±0·006	0·017±0·003*

$n=6$, *$P\leq 0{\cdot}05$. Percent BV/TV, bone volume/total volume; Tb. Th, trabecular thickness; Nob/BPm, number of osteoblasts/bone perimeter; Noc/BPm, number of osteoclasts/bone perimeter; ES/BS, eroded surface/bone surface; MS/BS, mineral surface/bone surface; MAR, mineral apposition rate; BFR/BS, bone formation rate/bone surface.

bone volume/total volume (percent BV/TV) in both the female and male *Irs1*$^{sml/sml}$ mice compared with the controls (Table 3). For the female mutants, this 73% reduction in BV/TV was accompanied by a 33% decrease in trabecular number and a 42% reduction in trabecular thickness. However, the male mutants' distal femoral percent BV/TV was only reduced by 29% when compared with the controls. This gender difference was attributed to a 20% increase in trabecular number in the *Irs1*$^{sml/sml}$ male femurs. Although, increased in number, these trabeculae were 34% thinner than those of the controls (Table 3).

Comparison of the *Irs1*$^{+/sml}$ female and male bones with those of the *Irs1*$^{+/+}$ and *Irs1*$^{sml/sml}$ mice revealed a significant intermediate phenotype for femur length, vBMD, and periosteal circumference (Table 3). Likewise, a significant intermediate phenotype was found at the mid-shaft for cortical thickness and percent BA/TA as measured by MicroCT. Interestingly, the heterozygous genotype did not affect percent BV/TV or trabecular number in the distal femur compartment, although a slight but significant reduction in trabecular thickness was observed when compared with the *Irs1*$^{+/+}$ controls (Table 3).

Histomorphometry

Histomorphometry from the distal femur of male and female *Irs1*$^{+/+}$ and *Irs1*$^{sml/sml}$ mice at 13 weeks of age showed a marked and significant decrease in the percent BV/TV analogous to what was observed by MicroCT. For both genders, the *Irs1*$^{sml/sml}$ mice had markedly reduced mineralizing surface/bone surface (percent MS/BS), mineral apposition rate (MAR), and bone formation rate (BFR). Furthermore, the numbers of osteoblasts and osteoclasts per bone perimeter (Nob/BPm and Noc/BPm) were increased in both genders of *Irs1*$^{sml/sml}$ mice compared with the *Irs1*$^{+/+}$ controls. However, this increase was only significant for *Irs1*$^{sml/sml}$ females (Table 4). Remarkably, there was no evidence of marrow adiposity in the histological sections of the *Irs1*$^{sml/sml}$ femurs compared with the *Irs1*$^{+/+}$ femurs (Supplementary Figure 1, see section on supplementary data given at the end of this article). Inspection of the growth plate in the proximal femur revealed a marked reduction in thickness in the *Irs1*$^{sml/sml}$ mice compared with the *Irs1*$^{+/+}$ mice, which was consistent with their reduced bone length (Fig. 2). The *Irs1*$^{+/sml}$ growth plate was also mildly reduced compared with the *Irs1*$^{+/+}$ mice.

Bone volume fraction by histomorphometry in the *Irs1*$^{+/sml}$ female mice at 13 weeks of age was not different from percent BV/TV in the *Irs1*$^{+/+}$ mice, akin to the findings by MicroCT. However, osteoclast numbers per bone perimeter were significantly increased ($P<0{\cdot}05$) in the *Irs1*$^{+/sml}$ heterozygote mice compared with the *Irs1*$^{+/+}$ females, and there was a significant ($P<0{\cdot}05$) reduction in MAR, although no statistical differences were noted in the overall BFRs nor eroded surfaces/bone surface (see Supplementary Table S1, see section on supplementary data given at the end of this article).

Cell culture

Alkaline phosphatase (ALP) staining of bone marrow stromal cell cultures of both male and female *Irs1*$^{sml/sml}$ mice on day 7 in culture revealed reductions in the number of CFU-ALP+ pre-OBs compared with the *Irs1*$^{+/+}$ cultures. Similarly, on days 18 and 24, the amount of ALP staining and mineral visually detected by von Kossa staining were less in the *Irs1*$^{sml/sml}$ mice than in the *Irs1*$^{+/sml}$ heterozygotes, and both were less than those detected in the *Irs1*$^{+/+}$ control cultures (Fig. 3). When non-adherent marrow cells were cultured in m-CSF and RANKL, no differences in tartrate-resistant acid phosphatase-positive multinucleated cells were seen among mutant, heterozygote, or control mice (Fig. 3).

To determine if the increased osteoclast number in the *Irs1*$^{sml/sml}$ mice as noted by histomorphometry was related to

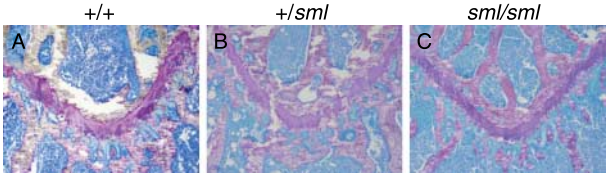

Figure 2 Toluidine blue staining of the proximal femur growth plate at 10× magnification of 13-week-old *Irs1*$^{+/+}$, *Irs1*$^{+/sml}$, and *Irs1*$^{sml/sml}$ mice.

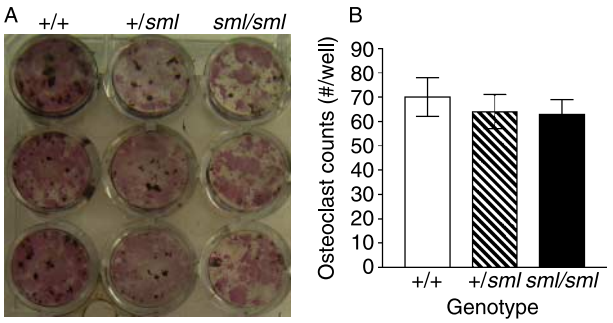

Figure 3 Bone marrow stromal cultures (BMSCs) of $Irs1^{sml/sml}$, $Irs1^{+/sml}$, and $Irs1^{+/+}$ control females. (A) On day 18, adherent OB progenitor cells were identified by alkaline phosphatase staining (CFU-ALP) and mineralization was identified by von Kossa staining. (B) Numbers of osteoclast cells in the bone marrow stromal cultures of $Irs1^{sml/sml}$, $Irs1^{+/sml}$, and $Irs1^{+/+}$ mice. On day 7, the cells were fixed and stained for TRAP5b. TRAP5b-positive multinucleated (>3 nuclei) osteoclasts were then counted using light microscopy. In all the experiments, male BMSCs exhibited a pattern that was similar to that exhibited by the females. Full colour version of this figure available via http://dx.doi.org/10.1677/JOE-09-0328.

the secretion of osteoclastogenic cytokines, we measured RANKL and OPG (listed as TNFRSF11B in the MGI Database) expression in calvarial osteoblasts and in 8-week-old femoral samples from the $Irs1^{sml/sml}$ and $Irs1^{+/+}$ controls. There were no statistical differences in RANKL expression by real-time PCR between mutants and controls from either site. Similarly for OPG, no strain differences were noted in calvarial osteoblast expression of *Opg* (*Tnfrs11b*) mRNA, although in the femoral samples from the $Irs1^{sml/sml}$ mice, there was a modest but non-significant (~10%) reduction in OPG expression by real-time PCR compared with the controls.

Western blot analysis of the protein isolated from calvarial osteoblast cultures revealed that at baseline, both the $Irs1^{+/sml}$ and $Irs1^{sml/sml}$ cultures had significantly less pAKT compared with the $Irs1^{+/+}$ control cultures (Fig. 1B). Upon stimulation with IGF1 or insulin, tAKT protein was the same across the genotypes, but the $Irs1^{+/+}$ cultures showed higher levels of AKT phosphorylation than the $Irs1^{sml/sml}$ and the $Irs1^{+/sml}$ cells. Finally, we examined the amount of IRS2 in calvarial osteoblasts from $Irs1^{+/+}$, $Irs1^{+/sml}$, and $Irs1^{sml/sml}$ mice. Although total protein was the same for all the three genotypes, both $Irs1^{sml/sml}$ and $Irs1^{+/sml}$ calvarial osteoblasts showed enhanced phosphorylation of IRS-2 in response to IGF1 but not to insulin (Fig. 4) compared with the $Irs1^{+/+}$ osteoblasts.

Serum analysis

Circulating levels of insulin and IGF1 were analyzed under fasting conditions. $Irs1^{sml/sml}$ mice were found to be relatively hyperinsulinemic, with 3·5- to 4-fold higher insulin levels compared with the $Irs1^{+/+}$ controls. Notably, heterozygous $Irs1^{+/sml}$ mice of both genders exhibit an intermediate phenotype marked by significantly higher serum levels of insulin compared with the $Irs1^{+/+}$ controls, but lower insulin levels compared with the $Irs1^{sml/sml}$ mice (Fig. 5A). Serum IGF1 levels were modestly, but significantly reduced in the $Irs1^{sml/sml}$ mice relative to the controls. In addition, a gender effect was observed in the serum IGF1 levels such that the heterozygous $Irs1^{+/sml}$ and $Irs1^{sml/sml}$ serum IGF1 levels were significantly lower in the females than in the males of the same genotype ($P<0{\cdot}0005$). Unexpectedly, there was no intermediate phenotype for the $Irs1^{+/sml}$ males. However, in the female $Irs1^{+/sml}$ mice, we observed the same intermediate phenotype for serum IGF1 seen in the previous phenotypic datasets (Fig. 5B).

GTT and ITT

To investigate whether the mild hyperinsulinemia in $Irs1^{sml/sml}$ mice was indicative of a pre-diabetic state, GTTs were performed on fasted $Irs1^{+/+}$, $Irs1^{+/sml}$, and $Irs1^{sml/sml}$ males and females at 8 weeks of age (Fig. 5C and D). At baseline, $Irs1^{sml/sml}$ mice exhibited significantly lower (30–40%) fasting glucose levels compared with the controls (Fig. 5C). When challenged with glucose, $Irs1^{sml/sml}$ glucose values rose as expected, but remained significantly lower than either $Irs1^{+/+}$ or $Irs1^{+/sml}$ levels throughout the study. Although baseline glucose levels differed, glucose levels peaked 20 min post injection in $Irs1^{sml/sml}$ mice, as in both $Irs1^{+/+}$ or $Irs1^{+/sml}$ mice, and the rate of glucose metabolism was similar among all the three genotypes of mice.

For the ITT under non-fasting conditions, the $Irs1^{sml/sml}$ glucose levels decreased, but not to the full extent as seen in

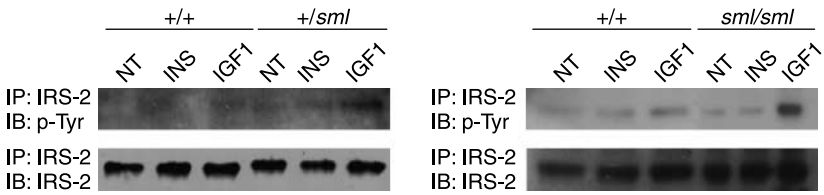

Figure 4 Mouse calvarial osteoblast cultures from $Irs1^{sml/sml}$, $Irs1^{+/sml}$, and $Irs1^{+/+}$ mice were treated with IGF1 (IGF1) and insulin (INS) or were given no treatment (NT), harvested, and lysed as described in the Materials and Methods. Lysates were immunoprecipitated with an IRS-2 antibody and were then immunoblotted with IRS-2 for total protein levels or p-Tyr for phosphorylation of IRS-2.

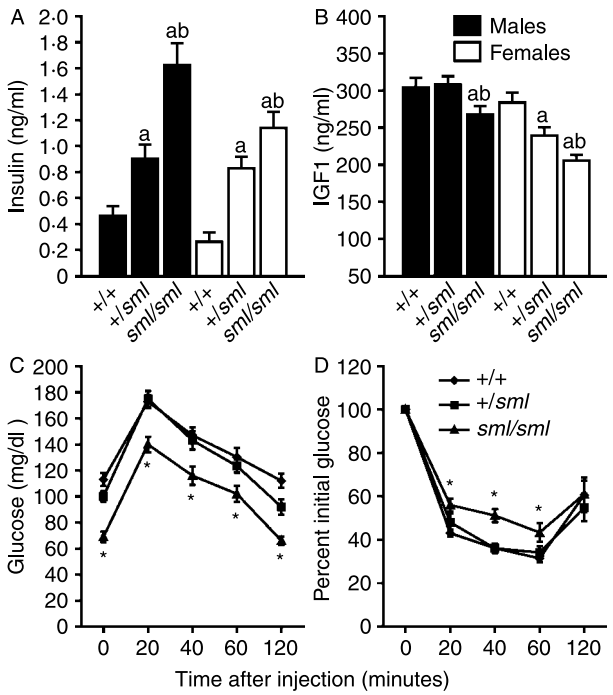

Figure 5 Fasted serum insulin and IGF1 levels and the glucose/insulin tolerance tests of $Irs1^{sml/sml}$, $Irs1^{+/sml}$, and $Irs1^{+/+}$ fasted mice during the glucose and insulin tolerance tests. At 16 weeks of age, males and females were tested for (A) insulin and (B) IGF1 serum levels (n=10 per genotype $^{*}P\leq0{\cdot}05$ $Irs1^{+/sml}$ versus $Irs1^{+/+}$, $^{**}P\leq0{\cdot}05$ $Irs1^{sml/sml}$ versus $Irs1^{+/+}$, and $^{***}P\leq0{\cdot}05$ $Irs1^{sml/sml}$ versus $Irs1^{+/sml}$). Male $Irs1^{+/+}$, $Irs1^{+/sml}$, and $Irs1^{sml/sml}$ mice at 8 weeks of age were fasted overnight and then subjected to a (C) GTT or fed *ad libitum* and then subjected to a (D) ITT as described in the Materials and Methods. Females were tested at the same time and they showed a similar pattern of significance (n=10 per genotype $^{*}P\leq0{\cdot}05$).

either $Irs1^{+/+}$ or $Irs1^{+/sml}$ mice. The glucose-lowering effect of insulin, as assessed by an ITT (Fig. 5D), revealed a mild insulin insensitivity, which was depicted as a slight, but significant, upward shift in the curve for $Irs1^{sml/sml}$ mice, relative to either $Irs1^{+/+}$ or $Irs1^{+/sml}$ mice (at 20-, 40-, and 60-min intervals). By 2 h post injection of insulin, $Irs1^{sml/sml}$ glucose levels were comparable to those of the $Irs1^{+/+}$ and $Irs1^{+/sml}$ mice.

Discussion

In this study, we have characterized for the first time a spontaneous mutation in the *Irs1* gene that results in a pronounced metabolic and skeletal phenotype. The $Irs1^{sml}$ mutation is a spontaneous frameshift mutation that results from a single nucleotide deletion in the *Irs1* gene leading to a premature stop codon and a truncated protein. This results in a hyperinsulinemic, lean, small mouse with reductions in serum IGF1 levels, BMD, and hearing. Mutant mice, although hyperinsulinemic, were only mildly insulin resistant as exogenous insulin treatment was effective in reducing circulating glucose levels. This partial ability of $Irs1^{sml/sml}$ mice to respond to exogenous insulin most likely prevents the development of overt hyperglycemia or diabetes.

The skeletal phenotype of the $Irs1^{sml/sml}$ mice is remarkable and differs from that of the genetically engineered *Irs1* null mice. $Irs1^{sml/sml}$ bones exhibited reductions in femur length, cortical and trabecular thicknesses, and trabecular number. In addition, $Irs1^{sml/sml}$ mice had a pronounced reduction in MAR and BFRs. But unexpectedly, these mutants had more osteoclasts and more osteoblasts per bone perimeter than the controls. To understand the mechanism for this surprising finding, we performed *in vitro* studies which demonstrated that $Irs1^{sml/sml}$ osteoblasts had impaired cell proliferation and differentiation, but no differences were found in osteoclast recruitment, differentiation, or appearance. Histological sections demonstrated that there was adequate recruitment of osteoblast precursors; hence the defect in bone formation was likely a result of poor osteoblast function due to reduced IRS-1 signaling. Taken together, we postulate that the markedly reduced bone volume fraction in the $Irs1^{sml/sml}$ mice is due to the inability of osteoblasts to form new bone coupled to an increase in osteoclastic activity, as evident by the larger eroded surfaces and the greater number of osteoclasts in the $Irs1^{sml/sml}$ mice. The absence of an *in vitro* effect on osteoclast differentiation from this mutation (see Fig. 3B) suggests that the osteoclastic changes are due to a non-cell autonomous process. In preliminary studies using real-time PCR on femoral and calvarial samples, we were unable to detect differences in gene expression for *RANKL*, but we did find slightly lower *Opg* mRNA in the $Irs1^{sml/sml}$ bones versus $Irs1^{+/+}$ controls. Whether the enhanced osteoblast recruitment is a compensatory response to a major defect in differentiative osteoblast function or another process remains to be determined. But, interestingly, Zhang *et al.* (2002) reported that mice with a conditional *Igf1r* deletion in osteoblasts exhibited defective mineralization, and had markedly increased osteoblast numbers. This would imply there must be feedback signals that operate during terminal differentiation that attempt to compensate for impaired skeletal function.

Similarities and differences exist between this spontaneous mutation and two genetically engineered mice, $Irs1^{tm1Tka}$ and $Irs1^{tm1Jos}$ with knockout alleles. For example, much like the $Irs1^{sml}$ mutation, the $Irs1^{tm1Tka}$ and $Irs1^{tm1Jos}$ null mutations result in small, lean, hyperinsulinemic mice, while the $Irs1^{tm1Tka}$ mice have reduced aBMD. Differences in phenotypes between the spontaneous $Irs1^{sml/sml}$ and the engineered $Irs1^{tm1Tka/tm1Tka}$ and $Irs1^{tm1Jos/tm1Jos}$ null mice include the lack of gender and heterozygous effects, as well as the degree of insulin resistance. Comparison of the spontaneous mutant to the $Irs1^{tm1Tka}$ allele also revealed differences in osteoblast and osteoclast numbers *in vivo* versus +/+ controls (Araki *et al.* 1994, Tamemoto *et al.* 1994, Ogata *et al.* 2000).

Phenotypic differences between the $Irs1^{tm1Tka/tm1Tka}$, $Irs1^{tm1Jos/tm1Jos}$, and the $Irs1^{sml/sml}$ mice may be the result of

the different background strains. Reports have alluded to the importance of genetic background-contributing alleles that alter bone and growth phenotypes in mutants (Gonzalez *et al.* 1992, Bouxsein *et al.* 2002, Martelli *et al.* 2005). The genetically engineered *Irs1* null models are reported to be on a hybrid B6/CBA background strain, whereas the $Irs1^{sml}$ spontaneous mutation is on an inbred C3.SWR-$H2^{b}$/SnJ congenic strain, which contains *C3H* alleles at all genetic regions except for a small fixed region on chromosome 17 carrying the *H2* allele. Thus, this background is more uniform compared with the segregating B6/CBA hybrid background. Modifier alleles within either background may account for the phenotypic variations observed between nulls and the spontaneous mutation.

Gender effects were not mentioned in the initial studies of the $Irs1^{tm1Tka/tm1Tka}$ and the $Irs1^{tm1Jos/tm1Jos}$ mice. Further characterization of the $Irs1^{tm1Tka/tm1Tka}$ mice reported no apparent differences by gender in serum IGF1 levels or in skeletal phenotyping (Ogata *et al.* 2000). However, phenotypic characterization of the $Irs1^{sml}$ mutation revealed gender differences for circulating IGF1, microarchitectural characteristics of bone, and osteoblast and osteoclast numbers by histomorphometry. In fact, $Irs1^{tm1Tka/tm1Tka}$ males are reported to have decreased numbers of both osteoblasts and osteoclasts (Hoshi *et al.* 2004, Yamaguchi *et al.* 2005), while the $Irs1^{sml/sml}$ male mice had normal numbers of both, and $Irs1^{sml/sml}$ female mice actually had more osteoblasts and osteoclasts. The gender effects are likely to be complex, but they may be a consequence of interactions involving estrogen, IGF1 signaling, and bone turnover.

Ogata *et al.* (2000) reported no phenotypic differences between the heterozygous and +/+ controls in the $Irs1^{tm1Tka/tm1Tka}$ nulls. The $Irs1^{+/sml}$ mice on the other hand exhibited a heterozygous phenotype for body weight, serum insulin, IGF1, femur length, aBMD and vBMD, and body fat. Moreover, the $Irs1^{+/sml}$ calvarial osteoblasts had some impairment in the phosphorylation of AKT that could explain the phenotypic changes. Furthermore, closer examination of bone microstructure revealed a heterozygous phenotype for the cortical compartment, such that the $Irs1^{+/sml}$ mice exhibited an intermediate phenotype for cortical thickness and periosteal circumference, but not for the trabecular compartment for bone volume fraction (See Table 2). On dynamic histomorphometry, the $Irs1^{+/sml}$ mice also had increased numbers of osteoclasts and reduced MAR compared with the controls (see Supplementary Table S1), suggesting that the heterozygote mice truly exhibit an intermediate phenotype for several components of skeletal turnover. It is interesting to speculate as to why the cortical component but not the trabecular component of the skeleton is affected by gene dosing. One possibility is that the increase in resorption in the heterozygotes is not as dramatic as that in the mutants, and this combined with minimal alterations in BFRs results in barely detectable changes in the trabecular bone volume fraction of $Irs1^{+/sml}$ mice. In contrast, despite body composition change in the $Irs1^{+/sml}$ mice, there was no intermediate metabolic phenotype when the mice were challenged with glucose or insulin. Although no heterozygous phenotype was reported for the bones of $Irs1^{tm1Tka/tm1Tka}$ mice, a study done by Pete *et al.* (1999) did report small but significant reductions in body and organ weight in heterozygous $Irs1^{+/tm1Jos}$ mice. Once again, it is likely that these strain differences could be related to the background of the mice and/or any compensatory effect of IRS-2 (see Fig. 4) that might result from the loss of a single allele in the *Irs1* gene.

Numerous studies have provided evidence of hyperinsulinemia, impaired glucose tolerance, and insulin resistance in *Irs1* null mice (Araki *et al.* 1994, Tamemoto *et al.* 1994, Yamauchi *et al.* 1996, Kido *et al.* 2000). Initial studies on both $Irs1^{tm1Tka/tm1Tka}$ and $Irs1^{tm1Jos/tm1Jos}$ mice reported normal physiological glucose levels after fasting conditions. However, upon glucose challenge, $Irs1^{tm1Jos/tm1Jos}$ mice were reported to be somewhat glucose intolerant as their circulating glucose levels significantly increased compared with the +/+ controls, whereas the $Irs1^{tm1Tka/tm1Tka}$ mice were reported to have no differences compared with the +/+ controls. When $Irs1^{tm1Jos/tm1Jos}$ and $Irs1^{tm1Tka/tm1Tka}$ mice were challenged with insulin, significantly increased levels of glucose were observed again in both the groups compared with the controls, indicating insulin resistance. The $Irs1^{sml/sml}$ mice, on the other hand, exhibited a compensatory hyperinsulinemia due to the lack of IRS1, but retained some insulin sensitivity, as shown by their nearly intact response to the glucose-lowering effects of exogenous insulin. Furthermore, the $Irs1^{sml/sml}$ mice exhibited one-third lower glucose levels after fasting and throughout the GTT. This attenuated glucose response can be explained by the moderate hyperinsulinemia found in $Irs1^{sml/sml}$ mice.

Initial characterizations of the $Irs1^{tm1Tka/tm1Tka}$ mice reported no significant differences in serum IGF1 levels (Tamemoto *et al.* 1994). However, Pete *et al.* (1999) reported a decrease in IGF1 levels in $Irs1^{tm1Jos/tm1Jos}$ mice compared with the controls, but the change did not reach significance, most likely due to low sampling numbers. In the spontaneous $Irs1^{sml/sml}$ mice, there was a consistent 20% decrease in IGF1 levels compared with the $Irs1^{+/+}$ control mice. Dong *et al.* (2006) also reported a 20% decrease in IGF1 levels in the $Irs1^{tm1Jos/tm1Jos}$ mouse compared with the controls. The 20% reduction in the IGF1 serum levels in the $Irs1^{sml/sml}$ mice is an unexpected observation. A defect in signaling should result in increased IGF1 levels rather than in a decrease, presumably as a compensatory mechanism. It is probable that the overexpression of IGF1 could partially compensate for the lack of IRS1 in postnatal growth (Pete *et al.* 1999). However, we postulate the emergence of a negative feedback loop in the absence of IRS1 that leads to reduced IGF1 synthesis. How that inhibition occurs (perhaps locally by alterations in GH signaling) is a subject of further investigations.

We assume that the $Irs1^{sml}$ mutation results in complete loss of function, but cannot rule out the possibility of a hypomorphic mutation. Indeed, it is possible that a

211-amino acid truncated peptide is produced and may bind to the IGF1 receptor by its phosphotyrosine-binding (PTB) domain. If so, all the sites of binding and phosphorylation downstream of the PTB domain are missing resulting in defective signaling as evidenced by the lack of AKT phosphorylation in mouse calvarial osteoblast cells when stimulated with IGF1 or insulin. This deleted region includes serine residues, which when phosphorylated, trigger protein degradation. Thus, it is possible that the truncated peptide may attach to the IGF1 receptor and perturb the system, resulting in the phenotypic differences observed between our spontaneous mutant and the engineered mutants of the *Irs1* gene. Repeated attempts to use the only commercially available N-terminus-specific antibody were unsuccessful. However, since the PTB domain of the IRS1 protein comprises residues 144–316, our predicted protein would contain <50% of the PTB domain, and thus binding to the receptor is unlikely.

Reduced circulating IGF1 and mutations in the *Igf1* gene have been directly linked to hearing loss in both mice and humans (Woods *et al.* 1996, Camarero *et al.* 2001, Barrenäs *et al.* 2003, Bonapace *et al.* 2003, Cediel *et al.* 2006). Mice lacking the *Igf1* gene have been shown to lose many auditory neurons and exhibit increased auditory thresholds indicative of hearing impairment (Camarero *et al.* 2001, Cediel *et al.* 2006). It has also been shown that IGF1 is critical in the development of the cochleovestibular ganglion in the inner ear (Varela-Nieto *et al.* 2004). Furthermore, lack of IGF1, or mutations in the *IGF1* gene, has been associated with sensorineural hearing loss in humans (Woods *et al.* 1996, Bonapace *et al.* 2003). Thus, the fact that $Irs1^{sml}$ mice exhibit hearing loss further supports the existence of a major defect in the IGF1 signaling pathway.

Recently, a SNP located adjacent to the *Irs1* gene has been associated with type 2 diabetes, insulin resistance, and hyperinsulinemia in a human cohort of more than 14 000 individuals. The investigators reported a 40% reduction in the basal levels and function of IRS1 protein in the skeletal muscle of patients carrying this variant (Rung *et al.* 2009). Likewise, there are numerous studies on humans demonstrating polymorphisms in the *Irs1* gene associated with variable responsiveness to insulin signaling (Imai *et al.* 1994, Ura *et al.* 1996, Le Fur *et al.* 2002). The most common polymorphism, the G972R variant, has also been associated with type II diabetes mellitus (Almind *et al.* 1993, Sesti 2000, Tok *et al.* 2006). However, there are no data examining the relationship between these polymorphisms and BMD or fracture risk. Based on our work combined with previous studies performed on the *Irs1* knockout models, we predict that patients with IRS1 polymorphisms could have a subclinical but important skeletal phenotype.

There are several limitations of our studies. First, the mechanism responsible for the low serum IGF1 levels in the $Irs1^{sml/sml}$ mice is not readily apparent from our data. Secondly, the degree of compensation between IRS1 and IRS2 in the mutant and heterozygote models requires further study. Thirdly, the hyperinsulinemia along with the mild insulin resistance phenotype is intriguing and raises new questions about the importance of IRS1 in glucose homeostasis. Fourthly, the heterozygous phenotype is particularly provocative as it lends credence to the theory that similar mutations in the *Irs1* gene may exist in humans. These are likely to be characterized by relatively modest reductions of IGF1, low fat mass, hyperinsulinemia, reduced BMD, and short stature. However, this theory will need to be verified in large population studies. Finally, the increase in osteoclastogenesis in both the mutant and heterozygote mice requires further study to determine if the relatively modest reduction in *Opg* mRNA in the pre-osteoblasts of these mice is partly responsible for the skeletal phenotype. Notwithstanding, this paper reports the first spontaneous 'loss of function' mutation in the *Irs1* gene. The unique phenotypic presentation of this mutant raises new questions about the role of IRS1 in both skeletal acquisition and glucose homeostasis.

Supplementary data

This is linked to the online version of the paper at http://dx.doi.org/10.1677/JOE-09-0328.

Declaration of interest

The authors declare that there is no conflict of interest that could be perceived as prejudicing the impartiality of the research reported.

Funding

This work was supported by the National Institute of Heath (grants: RR01183, ARMYLRD, DK042424, DK073267, AR46544, and AR043618).

Acknowledgements

The authors would like to thank Lindsay G Horton, Colleen Kane, Belinda Harris, Leona Gagnon, Krista Delahunty, Lisa Carney, Pat Ward-Bailey, and Cheryl Ackert-Bicknell for assistance with this research.

References

Almind K, Bjørbaek C, Vestergaard H, Hansen T, Echwald S & Pedersen O 1993 Aminoacid polymorphisms of insulin receptor substrate-1 in non-insulin-dependent diabetes mellitus. *Lancet* **342** 828–832.

Araki E, Lipes MA, Patti ME, Brüning JC, Haag B, Johnson RS & Kahn CR 1994 Alternative pathway of insulin signalling in mice with targeted disruption of the IRS-1 gene. *Nature* **10** 186–190.

Atti E, Boskey AL & Canalis E 2005 Overexpression of IGF-binding protein 5 alters mineral and matrix properties in mouse femora: an infrared imaging study. *Calcified Tissue International* **76** 187–193.

Barrenäs ML, Bratthall A & Dahlgren J 2003 The thrifty phenotype hypothesis and hearing problems. *BMJ* **327** 1199–2000.

Baumann G 1999 Mutations in the growth hormone releasing hormone receptor: a new form of dwarfism in humans. *Growth Hormone and IGF Research* **9** 24–29.

Beamer WG, Shultz KL, Ackert-Bicknell CL, Horton LG, Delahunty KM, Coombs HF III, Donahue LR, Canalis E & Rosen CJ 2007 Genetic dissection of mouse distal chromosome 1 reveals three linked BMD QTLs with sex-dependent regulation of bone phenotypes. *Journal of Bone and Mineral Research* **22** 1187–1196.

Ben Lagha N, Seurin D, Le Bouc Y, Binoux M, Berdal A, Menuelle P & Babajko S 2006 Insulin-like growth factor binding protein (IGFBP-1) involvement in intrauterine growth retardation: study on IGFBP-1 overexpressing transgenic mice. *Endocrinology* **147** 4730–4737.

Bikle D, Majumdar S, Laib A, Powell-Braxton L, Rosen C, Beamer W, Nauman E, Leary C & Halloran B 2001 The skeletal structure of insulin-like growth factor I-deficient mice. *Journal of Bone and Mineral Research* **16** 2320–2329.

Bonapace G, Concolino D, Formicola S & Strisciuglio P 2003 A novel mutation in a patient with insulin-like growth factor 1 (IGF1) deficiency. *Journal of Medical Genetics* **40** 913–917.

Bouxsein ML, Rosen CJ, Turner CH, Ackert LC, Shultz KL, Donahue LR, Churchill GA, Adamo ML, Powell DR, Turner RT *et al.* 2002 Generation of a new congenic mouse strain to test the relationships among serum insulin-like growth factor I, bone mineral density, and skeletal morphology *in vivo*. *Journal of Bone and Mineral Research* **17** 570–579.

Camarero G, Avendano C, Fernandez-Moreno C, Villar A, Contreras J, de Pablo F, Pichel JG & Varela-Nieto I 2001 Delayed inner ear maturation and neuronal loss in postnatal Igf-1 deficient mice. *Journal of Neuroscience* **21** 7630–7641.

Cediel R, Riquelme R, Contreras J, Díaz A & Varela-Nieto I 2006 Sensorineural hearing loss in insulin-like growth factor I-null mice: a new model of human deafness. *European Journal of Neuroscience* **23** 587–590.

Cornish J, Callon KE & Reid IR 1996 Insulin increases histomorphometric indices of bone formation *in vivo*. *Calcified Tissue International* **59** 492–495.

Delahunty KM, Shultz KL, Gronowicz GA, Koczon-Jaremko B, Adamo ML, Horton LG, Lorenzo J, Donahue LR, Ackert-Bicknell CL, Kream BE *et al.* 2006 Congenic mice provide *in vivo* evidence for a genetic locus that modulates serum insulin-like growth factor-1 and bone acquisition. *Endocrinology* **147** 3915–3923.

DeMambro VE, Clemmons DR, Horton LG, Bouxsein ML, Wood TL, Beamer WG, Canalis E & Rosen CJ 2008 Gender-specific changes in bone turnover and skeletal architecture in igfbp-2-null mice. *Endocrinology* **149** 2051–2061.

Donahue LR & Beamer WG 1993 Growth hormone deficiency in 'little' mice results in aberrant body composition, reduced insulin-like growth factor-I and insulin-like growth factor-binding protein-3 (IGFBP-3), but does not affect IGFBP-2, -1 or -4. *Journal of Endocrinology* **136** 91–104.

Dong X, Park S, Lin X, Copps K, Yi X & White MF 2006 Irs1 and Irs2 signaling is essential for hepatic glucose homeostasis and systemic growth. *Journal of Clinical Investigation* **116** 101–114.

Gagnon LH, Longo-Guess CM, Berryman M, Shin JB, Saylor KW, Yu H, Gillespie PG & Johnson KR 2006 The chloride intracellular channel protein CLIC5 is expressed at high levels in hair cell stereocilia and is essential for normal inner ear function. *Journal of Neuroscience* **26** 10188–10198.

Garnero P, Sornay-Rendu E & Delmas PD 2000 Low serum IGF-1 and occurrence of osteoporotic fractures in postmenopausal women. *Lancet* **355** 898–899.

Giustina A, Mazziotti G & Canalis E 2008 Growth hormone, insulin-like growth factors, and the skeleton. *Endocrine Reviews* **29** 535–559.

Godfrey P, Rahal JO, Beamer WG, Copeland NG, Jenkins NA & Mayo KE 1993 GHRH receptor of little mice contains a missense mutation in the extracellular domain that disrupts receptor function. *Nature Genetics* **4** 227–232.

Gonzalez CD, Meyer RAJ & Iorio RJ 1992 Craniometric measurements of craniofacial malformations in the X-linked hypophosphatemic (Hyp) mouse on two different genetic backgrounds: C57BL/6J and B6C3H. *Teratology* **46** 605–613.

He J, Rosen CJ, Adams DJ & Kream BE 2006 Postnatal growth and bone mass in mice with IGF-I haploinsufficiency. *Bone* **38** 826–835.

Hoshi K, Ogata N, Shimoaka T, Terauchi Y, Kadowaki T, Kenmotsu S, Chung UI, Ozawa H, Nakamura K & Kawaguchi H 2004 Deficiency of insulin receptor substrate-1 impairs skeletal growth through early closure of epiphyseal cartilage. *Journal of Bone and Mineral Research* **19** 214–223.

Imai Y, Fusco A, Suzuki Y, Lesniak MA, D'Alfonso R, Sesti G, Bertoli A, Lauro R, Accili D & Taylor SI 1994 Variant sequences of insulin receptor substrate-1 in patients with noninsulin-dependent diabetes mellitus. *Journal of Clinical Endocrinology and Metabolism* **79** 1655–1658.

Janghorbani M, Feskanich D, Willett WC & Hu F 2006 Prospective study of diabetes and risk of hip fracture: the Nurses' Health Study. *Diabetes Care* **29** 1573–1578.

Janghorbani M, Van Dam RM, Willett WC & Hu FB 2007 Systematic review of type 1 and type 2 diabetes mellitus and risk of fracture. *American Journal of Epidemiology* **166** 495–505.

Kido Y, Burks DJ, Withers D, Bruning JC, Kahn CR, White MF & Accili D 2000 Tissue-specific insulin resistance in mice with mutations in the insulin receptor, IRS-1, and IRS-2. *Journal of Clinical Investigation* **105** 199–205.

Le Fur S, Le Stunff C & Bougnères P 2002 Increased insulin resistance in obese children who have both 972 IRS-1 and 1057 IRS-2 polymorphisms. *Diabetes* **51** S304–S307.

Lienhard GE 1994 Insulin. Life without the IRS. *Nature* **372** 128–129.

Liu JP, Baker J, Perkins AS, Robertson EJ & Efstratiadis A 1993 Mice carrying null mutations of the genes encoding insulin-like growth factor I (Igf-1) and type 1 IGF receptor (Igf1r). *Cell* **75** 59–72.

Maheshwari HG, Silverman BL, Dupuis J & Baumann G 1998 Phenotype and genetic analysis of a syndrome caused by an inactivating mutation in the growth hormone-releasing hormone receptor: dwarfism of Sindh. *Journal of Clinical Endocrinology and Metabolism* **88** 4065–4074.

Manly KF, Cudmore RHJ & Meer JM 2001 Map Manager QTX, cross-platform software for genetic mapping. *Mammalian Genome* **12** 930–932.

Martelli F, Ghinassi B, Panetta B, Alfani E, Gatta V, Pancrazzi A, Bogani C, Vannucchi AM, Paoletti F, Migliaccio G *et al.* 2005 Variegation of the phenotype induced by the Gata1low mutation in mice of different genetic backgrounds. *Blood* **106** 4102–4113.

Messier C & Kent P 1995 Repeated blood glucose measures using a novel portable glucose meter. *Physiology & Behavior* **57** 807–811.

Mukherjee A, Murray RD & Shalet SM 2004 Impact of growth hormone status on body composition and the skeleton. *Hormone Research* **62** 35–41.

Niu T & Rosen CJ 2005 The insulin-like growth factor-I gene and osteoporosis: a critical appraisal. *Gene* **361** 38–56.

Ogata N, Chikazu D, Kubota N, Terauchi Y, Tobe K, Azuma Y, Ohta T, Kadowaki T, Nakamura K & Kawaguchi H 2000 Insulin receptor substrate-1 in osteoblast is indispensable for maintaing bone turnover. *Journal of Clinical Investigation* **105** 935–943.

Parfitt AM, Drezner MK, Glorieux FH, Kanis JA, Malluche H, Meunier PJ, Ott SM & Reckner RR 1987 Bone histomorphometry: standardization of nomenclature, symbols and units. Report of the ASBMR nomenclature committee. *Journal of Bone and Mineral Research* **2** 595–610.

Pete G, Fuller CR, Oldham JM, Smith DR, D'Ercole AJ, Kahn CR & Lund PK 1999 Postnatal growth responses to insulin-like growth factor I in insulin receptor substrate-1-deficient mice. *Endocrinology* **140** 5478–5487.

Räkel A, Sheehy O, Rahme E & LeLorier J 2008 Osteoporosis among patients with type 1 and type 2 diabetes. *Diabetes & Metabolism* **34** 193–205.

Rosen C, Churchill G, Donahue L, Shultz K, Burgess J, Powell D & Beamer W 2000 Mapping quantitative trait loci for serum insulin-like growth factor-1 levels in mice. *Bone* **27** 521–528.

Rosen CJ, Ackert-Bicknell CL, Adamo ML, Shultz KL, Rubin J, Donahue LR, Horton LG, Delahunty KM, Beamer WG, Sipos J *et al.* 2004 Congenic mice with low serum IGF-1 have increased body fat, reduced bone mineral density, and an altered osteoblast differentiation program. *Bone* **35** 1046–1058.

Rung J, Cauchi S, Albrechtsen A, Shen L, Rocheleau G, Cavalcanti-Proença C, Bacot F, Balkau B, Belisle A, Borch-Johnsen K *et al.* 2009 Genetic variant near IRS1 is associated with type 2 diabetes, insulin resistance and hyperinsulinemia. *Nature Genetics* **41** 1110–1115.

Sesti G 2000 Insulin receptor substrate polymorphisms and type 2 diabetes mellitus. *Pharmacogenetics* **1** 343–357.

Shimoaka T, Kamekura S, Chikuda H, Hoshi K, Chung UI, Akune T, Maruyama Z, Komori T, Matsumoto M, Ogawa W *et al.* 2004 Impairment of bone healing by insulin receptor substrate-1 deficiency. *Journal of Biological Chemistry* **279** 15314–15322.

Shirakami A, Toyonaga T, Tsuruzoe K, Shirotani T, Matsumoto K, Yoshizato K, Kawashima J, Hirashima Y, Miyamura N, Kahn CR *et al.* 2002 Heterozygous knockout of the IRS-1 gene in mice enhances obesity-linked insulin resistance: a possible model for the development of type 2 diabetes. *Journal of Endocrinology* **174** 309–319.

Silha JV, Mishra S, Rosen CJ, Beamer WG, Turner RT, Powell DR & Murphy LJ 2003 Perturbations in bone formation and resorption in insulin-like growth factor binding protein-3 transgenic mice. *Journal of Bone and Mineral Research* **18** 1834–1841.

Tamemoto H, Kadowaki T, Tobe K, Yagi T, Sakura H, Hayakawa T, Terauchi Y, Ueki K, Kaburagi Y, Satoh S *et al.* 1994 Insulin resistance and growth retardation in mice lacking insulin receptor substrate-1. *Nature* **372** 182–186.

Tok EC, Ertunc D, Bilgin O, Erdal EM, Kaplanoglu M & Dilek S 2006 Association of insulin receptor substrate-1 G972R variant with baseline characteristics of the patients with gestational diabetes mellitus. *American Journal of Obstetrics and Gynecology* **194** 868–872.

Ura S, Araki E, Kishikawa H, Shirotani T, Todaka M, Isami S, Shimoda S, Yoshimura R, Matsuda K, Motoyoshi S *et al.* 1996 Molecular scanning of the insulin receptor substrate-1 (IRS-1) gene in Japanese patients with NIDDM: identification of five novel polymorphisms. *Diabetologia* **39** 600–608.

Varela-Nieto I, Morales-Garcia JA, Vigil P, Diaz-Casares A, Gorospe I, Sánchez-Galiano S, Cañon S, Camarero G, Contreras J, Cediel R *et al.* 2004 Trophic effects of insulin-like growth factor-I (IGF-I) in the inner ear. *Hearing Research* **196** 19–25.

Vestergaard P, Jørgensen JO, Hagen C, Hoeck HC, Laurberg P, Rejnmark L, Brixen K, Weeke J, Andersen M, Conceicao FL *et al.* 2002 Fracture risk is increased in patients with GH deficiency or untreated prolactinomas – a case–control study. *Clinical Endocrinology* **56** 159–167.

Wang Y, Nishida S, Elalieh HZ, Long RK, Halloran BP & Bikle DD 2006 Role of IGF-I signaling in regulating osteoclastogenesis. *Journal of Bone and Mineral Research* **21** 1350–1358.

Weitgasser R, Gappmayer B & Pichler M 1999 Newer portable glucose meters – analytical improvement compared with previous generation devices. *Clinical Chemistry* **45** 1821–1825.

White MF 2003 Insulin signaling in health and disease. *Science* **302** 1710–1711.

Woods KA, Camacho-Hübner C, Savage MO & Clark AJ 1996 Intrauterine growth retardation and postnatal growth failure associated with deletion of the insulin-like growth factor I gene. *New England Journal of Medicine* **335** 1363–1367.

Yakar S, Liu JL, Stannard B, Butler A, Accili D, Sauer B & LeRoith D 1999 Normal growth and development in the absence of hepatic insulin-like growth factor I. *PNAS* **96** 7324–7329.

Yakar S, Rosen CJ, Bouxsein ML, Sun H, Mejia W, Kawashima Y, Wu Y, Emerton K, Williams V, Jepsen K *et al.* 2009 Serum complexes of insulin-like growth factor-1 modulate skeletal integrity and carbohydrate metabolism. *FASEB Journal* **23** 709–719.

Yamaguchi M, Ogata N, Shinoda Y, Akune T, Kamekura S, Terauchi Y, Kadowaki T, Hoshi K, Chung UI, Nakamura K *et al.* 2005 Insulin receptor substrate-1 is required for bone anabolic function of parathyroid hormone in mice. *Endocrinology* **146** 2620–2628.

Yamauchi T, Tobe K, Tamemoto H, Ueki K, Kaburagi Y, Yamamoto-Honda R, Takahashi Y, Yoshizawa F, Aizawa S, Akanuma Y *et al.* 1996 Insulin signaling and insulin actions in the muscles and livers of insulin-resistant, insulin receptor substrate 1-deficient mice. *Molecular and Cellular Biology* **116** 101–114.

Zhang M, Xuan S, Bouxsein ML, von Stechow D, Akeno N, Faugere MC, Malluche H, Zhao G, Rosen CJ, Efstratiadis A *et al.* 2002 Osteoblast-specific knockout of the insulin-like growth factor (IGF) receptor gene reveals an essential role of IGF signaling in bone matrix mineralization. *Journal of Biological Chemistry* **277** 44005–44012.

Zhang M, Faugere MC, Malluche H, Rosen CJ, Chernausek SD & Clemens TL 2003 Paracrine overexpression of IGFBP-4 in osteoblasts of transgenic mice decreases bone turnover and causes global growth retardation. *Journal of Bone and Mineral Research* **18** 836–843.

Received in final form 9 December 2009
Accepted 23 December 2009
Made available online as an Accepted Preprint
23 December 2009